R

Rhodopsin Activation in Lipid Membranes Based on Solid-State NMR Spectroscopy

Suchithranga M. D. C. Perera[1], Xiaolin Xu[2], Trivikram R. Molugu[1], Andrey V. Struts[1,3] and Michael F. Brown[1,2]
[1]Department of Chemistry and Biochemistry, University of Arizona, Tucson, AZ, USA
[2]Department of Physics, University of Arizona, Tucson, AZ, USA
[3]Laboratory of Biomolecular NMR, St. Petersburg State University, St. Petersburg, Russia

Definition

Rhodopsin is an archetype for a large class of membrane proteins called G-protein-coupled receptors (GPCRs) that are activated by diffusible small-molecule ligands or by light. Understanding their mechanisms of action requires information about both protein structure and dynamics within the lipid membrane, as well as changes undergone by molecular interactions with bound cofactors. Nuclear magnetic resonance (NMR) spectroscopy informs the average molecular structure through intermolecular distances and orientations obtained directly from the single- or multi-dimensional NMR spectra. The corresponding rates of motion are obtained from analysis of the nuclear spin relaxation times. Knowledge of the protein structure and dynamics acquired by solid-state NMR spectroscopy contributes new insights into the light-induced changes of rhodopsin that result in the process of visual signaling.

Introduction

Rhodopsin mediates the scotopic vision of vertebrates under low light conditions and is the archetype for the G-protein-coupled receptor (GPCR) proteins that regulate many of the vital functions of humans (Stevens et al. 2013; Latorraca et al. 2017; Koehl et al. 2018; Masureel et al. 2018; Perera et al. 2018). Despite that they are targets of more than 30% of known pharmaceuticals, however, most GPCR structures are currently unknown (Stevens et al. 2013). Conventional approaches are challenged by difficulties in crystallizing GPCRs for X-ray analysis (Salom et al. 2006; Wu et al. 2015; Perera et al. 2017) or the requirement for detergent solubilization in the case of high-resolution NMR spectroscopy (Nygaard et al. 2013). Notably, visual rhodopsin is one of few GPCRs for which X-ray structures in various states have been elucidated (Scheerer et al. 2008; Park et al. 2008; Choe et al. 2011; Standfuss et al. 2011). Rhodopsin has also been studied by Fourier transform infrared (FTIR) methods, which detect short-range local interactions (Mahalingam et al. 2008; Zaitseva et al. 2010; Struts et al. 2015a), and by solid-state ^{2}H NMR spectroscopy, which affords additional

G. C. K. Roberts, A. Watts (eds.), *Encyclopedia of Biophysics*,
https://doi.org/10.1007/978-3-642-35943-9_788-2

insights into rhodopsin activation in lipid membrane bilayers (Brown and Struts 2014; Xu et al. 2014; Struts et al. 2016). The angular restraints from ^{2}H NMR are complemented by solid-state ^{13}C NMR spectroscopy which gives short distance restraints (Spooner et al. 2002, 2003; Ahuja et al. 2009a; Kimata et al. 2016; Hu et al. 2017) and by site-directed spin-labeling experiments that are sensitive to longer distances (Altenbach et al. 2008; Van Eps et al. 2011). Knowledge of its activation mechanism is provided that is highly complementary to other biophysical methods. This entry describes the application of solid-state NMR methods for acquiring structural and dynamical information for the retinal ligand of rhodopsin in a membrane lipid environment (Struts et al. 2007, 2011a, 2015a). The solid-state NMR spectra provide knowledge of the retinal structure, whereas NMR relaxation methods yield information about its dynamics. Combining the results of solid-state ^{2}H NMR spectroscopy with FTIR, ^{13}C NMR, and spin-labeling methods thus allows a comprehensive picture of the activation mechanism for rhodopsin in the natural membrane state to be obtained (Struts et al. 2011b).

Dynamical Structure of Retinal Bound to Rhodopsin Is Revealed by Solid-State NMR Spectroscopy

Studies of aligned bilayers containing visual rhodopsin with specifically ^{2}H-labeled retinal (Fig. 1a, b) allow one to determine the orientation of the quadrupolar coupling tensor of deuterium nuclei (Struts et al. 2007) with respect to the membrane normal (vector $\mathbf{n_0}$ in Fig. 1c). Calculated orientations of the deuterated methyl groups can then be used for modeling of the retinal structure within the ligand-binding cavity of rhodopsin. For rapidly spinning methyl groups, the principal axis of the motionally averaged quadrupolar tensor coincides with the rotation (symmetry) axis for the methyl group M and thus determines the average angle between M and $\mathbf{n_0}$ (Fig. 1). Solid-state ^{2}H NMR spectra of rhodopsin and metarhodopsin-I (Meta-I) obtained for the various methyl groups are presented in Fig. 2a, b (Struts et al. 2007). The fitting parameters used in the simulations of the theoretical ^{2}H NMR spectra include the C–C^{2}H$_3$ methyl bond orientation, the width of the orientational distribution of the local membrane normal (mosaic spread), the residual deuterium quadrupolar coupling, and the NMR line broadening. Reduction of the quadrupolar interaction of deuterium nuclei with the electric field gradient (EFG) in the molecule occurs because of the fast spinning of the methyl groups and reorientation of their symmetry axis. The ^{2}H NMR line shape is calculated by randomly generating the angle of rotation of the rhodopsin molecule and the angle of deviation of the membrane normal from the average value, and subsequently averaging the spectra over all possible orientations (Struts et al. 2007). The above method has been applied to aligned membranes containing rhodopsin (Brown et al. 2010) or bacteriorhodopsin (Brown et al. 2007), as well as to aligned DNA fibers (Nevzorov et al. 1999). For rhodopsin, analysis of the angular-dependent, solid-state ^{2}H NMR spectra yields the following orientations of the retinal C5-, C9-, and C13-methyl groups with respect to the protein long axis: $70 \pm 3°$, $52 \pm 3°$, and $68 \pm 2°$ in the dark state and $72 \pm 4°$, $53 \pm 3°$, and $59 \pm 3°$ in the Meta-I state (Fig. 1) (Struts et al. 2007).

Solid-State NMR Structure of Retinal Within Rhodopsin Binding Pocket Entails Angular and Distance Restraints

Additionally, the orientational restraints provided by solid-state ^{2}H NMR spectroscopy of retinal within its rhodopsin binding pocket are complementary to ^{13}C rotational resonance distance measurements (Verdegem et al. 1999). Taken together, the orientational restrains from ^{2}H NMR and the distance restraints from ^{13}C NMR enable site-specific structural information to be acquired, as in the case of solution NMR spectroscopy (Cavanaugh et al. 2006). Magic-angle spinning (MAS) rotational resonance NMR utilizes the dipolar recoupling or magnetization transfer between nuclear spins that occurs when the rotation speed of the sample matches the difference in the isotropic chemical shifts of two nonequivalent nuclei. Both

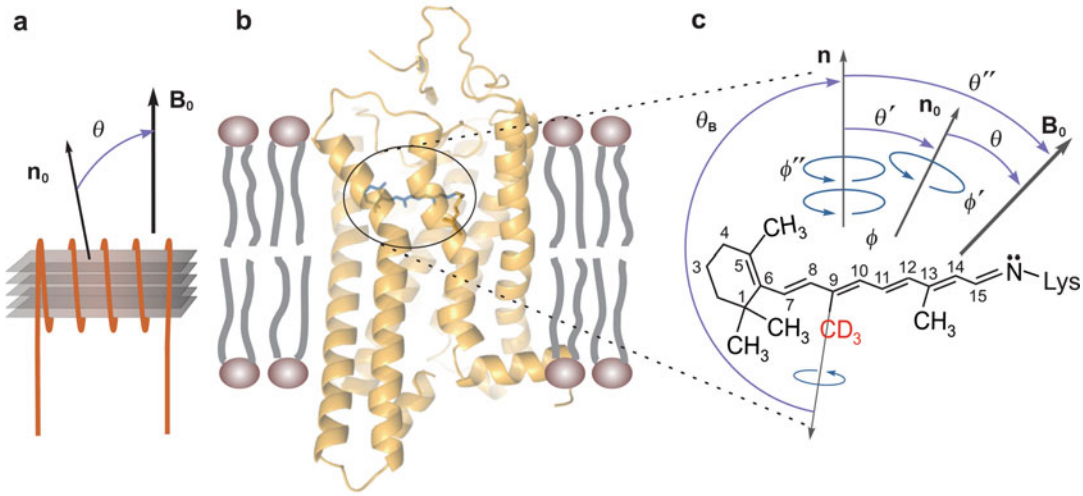

Rhodopsin Activation in Lipid Membranes Based on Solid-State NMR Spectroscopy, Fig. 1 Solid-state ^{2}H NMR spectroscopy investigates the structure and functional dynamics of retinal within the binding pocket of rhodopsin in a native-like membrane environment. (**a**) Illustration of stack of aligned membranes containing rhodopsin within the radiofrequency coil of the NMR spectrometer indicating geometry relative to the magnetic field. (**b**) Ribbon diagram of metarhodopsin-II (PDB code: 3PQR) showing seven transmembrane helices (yellow), with the N-terminus above (extracellular side) and C-terminus below (cytoplasmic side). (**c**) Chemical structure of all-*trans* retinylidene cofactor (Meta-II state); for an individual methyl group θ_B is angle of the C–C^{2}H$_3$ bond axis to the local bilayer normal **n**, with a static uniaxial distribution given by the azimuthal angle ϕ. Alignment disorder (mosaic spread) is characterized by the angle θ' of **n** to the average membrane normal $\mathbf{n_0}$ and is uniaxially distributed as described by ϕ'. The membrane tilt angle θ is from $\mathbf{n_0}$ to the static magnetic field $\mathbf{B_0}$ with cylindrical symmetry. Lastly θ'' is the angle from **n** to $\mathbf{B_0}$ where ϕ'' is the azimuthal angle. Theoretical analysis of geometry and ps–ns mobility of retinylidene methyl groups within the binding cavity of rhodopsin treats the rotational dynamics of methyl groups as axial threefold hops or continuous rotational diffusion (see text)

the NMR line splitting and magnetization exchange depend on the internuclear distance. The distance can be determined either by calibration with similar reference compounds, or by simulation of the NMR spectra or exchange curves (Spooner et al. 2002, 2003) with known NMR parameters (chemical shielding tensor, scalar coupling constant, zero-quantum spin-spin relaxation time).

As applied to rhodopsin, by using retinals doubly ^{13}C labeled at the C8–C16/C17, C8–C18, C10–C20, and C11–C20 positions, the conformation of the C10–C11=C12–C13–C20 motif and the rotation of the β-ionone ring versus the polyene chain have been examined in the dark and Meta-I states. The distances between carbons C10–C20 and C11–C20 calculated from ^{13}C rotational resonance NMR were 0.304 ± 0.015 nm and 0.293 ± 0.015 nm in the dark state and >0.435 nm and 0.283 ± 0.015 nm in the Meta-I state (Verdegem et al. 1999). Correspondingly, for carbons C8–C16/C17 and C8–C18, the distances were reported to be 0.405 ± 0.025 and 0.295 ± 0.015 nm in the dark state and effectively unchanged in the Meta-I state (Spooner et al. 2003). The twist for the C12–C13 bond was estimated to be 44 ± 10° in the dark state, and a relaxed all-*trans* retinal structure was observed in the Meta-I state (Verdegem et al. 1999). Additionally, it was established that the C5=C6–C7=C8 torsion angle characterizing the β-ionone ring orientation was −28 ± 7° in the dark state, and a similar orientation was revealed in the Meta-I state (Spooner et al. 2003).

Further investigation of the 3D retinal structure has been carried out within the framework of a three-plane model (Struts et al. 2007) (Fig. 2c). Within each of the three planes (A, B, and C), deviation of the torsion angles from the ideal 11-*cis* or all-*trans* configuration was neglected (the polyene chain was assumed to be flat within

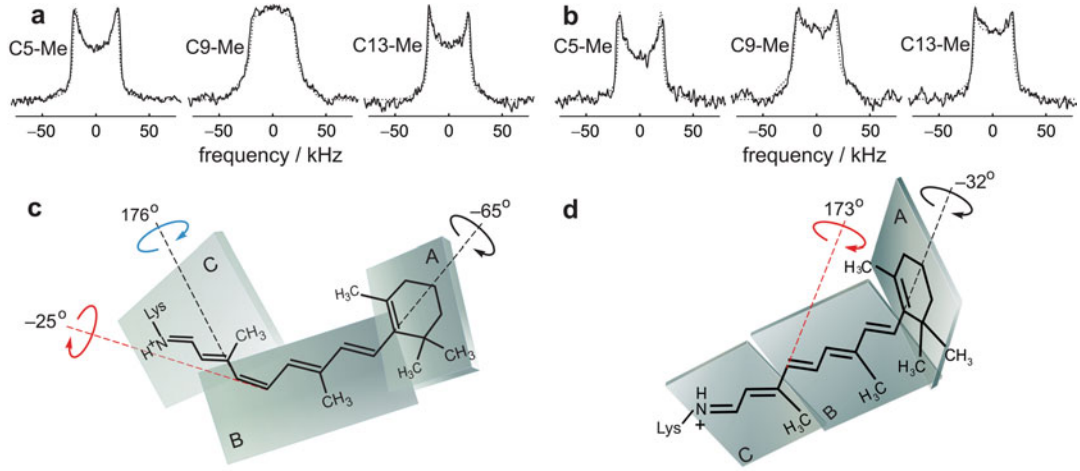

Rhodopsin Activation in Lipid Membranes Based on Solid-State NMR Spectroscopy, Fig. 2 Solid-state ^{2}H NMR spectroscopy characterizes the structure of the retinal ligand bound to rhodopsin. Examples of solid-state ^{2}H NMR spectra for (**a**) dark and (**b**) Meta-I states of rhodopsin regenerated with 11-*cis* retinal specifically ^{2}H-labeled at C5-, C9-, or C13-methyl positions in aligned POPC membranes (1:50 molar ratio). The spectra are measured for the orientation of the membrane normal parallel to the magnetic field at temperatures of −150 and −100 °C for rhodopsin and Meta-I, respectively. (**c**) The solid-state NMR structure proposed for retinal in the dark state of rhodopsin. (**d**) The solid-state NMR structure proposed for retinal in Meta-I. Rhodopsin orientation is with the C-terminus above (cytoplasmic side) and the N-terminus below (extracellular side) to facilitate comparison with published X-ray structures. (Adapted with permission from (Brown and Struts 2014))

the planes). Only torsion angles between the different planes were allowed to deviate (Fig. 2c). Comparison of the ^{2}H NMR structure with crystallographic data indicates that such a model corresponds well to the X-ray structure of retinal within the binding pocket of rhodopsin in the dark state (Struts et al. 2007; Brown and Struts 2014). Notably, the methyl group orientations are obtained directly from the NMR line shape; they are not related to the above model ("model-free"), and hence they can be juxtaposed directly with the crystallographic results. Such a comparison establishes a very good agreement between the ^{2}H NMR (Struts et al. 2007) and the X-ray data (Okada et al. 2004).

Deuterium NMR of Rhodopsin in Aligned Bilayers Reveals Torsional Twisting of Retinal Chromophore

Next, returning back to Fig. 2, we can see that the three planes used for the retinal modeling (Struts et al. 2007) encompass the β-ionone ring (plane A) and the polyene chain on both sides of the C12–C13 bond (planes B and C). For retinal bound to rhodopsin in aligned membrane bilayers, the methyl group orientations calculated from the orientation-dependent ^{2}H NMR line shapes provide a set of angular restraints that allow one to determine the dihedral angles between the planes, together with the orientation of the retinal ligand with respect to the rhodopsin molecule. In mathematical closed form, our calculations have shown that the torsion angle $\chi_{i,k}$ between two planes having a common bond C_i–C_k is given by (Salgado et al. 2004; Struts et al. 2007

$$\chi_{i,k} = \cos^{-1}\left(\frac{\cos\theta_i \cos\theta_B^{i,k} - \cos\theta_B^i}{\sin\theta_i \sin\theta_B^{i,k}}\right) - \cos^{-1}\left(\frac{\cos\theta_k \cos\theta_B^{i,k} - \cos\theta_B^k}{\sin\theta_k \sin\theta_B^{i,k}}\right) \quad (1)$$

In the above formula, θ_B^i and θ_B^k are the orientations of the individual methyl group axes with respect to the membrane normal, and θ_i and θ_k

are the angles of the two methyl axes relative to the C_i–C_k bond. Moreover, the C_i–C_k bond angle to the membrane normal is $\theta_B^{i,k}$, and it is calculated from the C9-methyl orientation together with the orientation of the electronic transition dipole moment (Struts et al. 2007).

To continue further, the orientations of the methyl groups from ^{2}H NMR spectroscopy and the orientation of the electronic transition dipole moment from polarized UV-visible spectroscopy (Jäger et al. 1997) are introduced as combined angular restraints (Struts et al. 2007). The distances between carbons C10–C20 and carbons C11–C20 calculated from ^{13}C NMR results (Verdegem et al. 1999) are introduced as additional geometrical constraints in the extended model. By using this approach, various solutions were obtained for the torsion angles between the planes A, B, and C, providing 64 combinations for the relative orientations of the planes and 128 configurations and orientations for retinal within the ligand-binding cavity (Struts et al. 2007). Even so, most of these solutions can be discarded, as they do not satisfy the ^{13}C NMR distance constraints between the atoms C8–C18, C8–C16/C17 (Spooner et al. 2003), C10–C20, and C11–C20 (Verdegem et al. 1999), as well as the signs of the torsion angles obtained from circular dichroism (CD) measurements (Fujimoto et al. 2002). The resulting ^{2}H NMR retinal structure in the dark state is shown in Fig. 2c (Struts et al. 2007). One distinguishing feature is the twist around the C11=C12 bond; attempts to calculate the retinal structure without the twist failed, because the retinal moiety does not fit into the binding cavity of the rhodopsin crystal structure. This proposal of a pretwist in the direction of the isomerization can help to explain the ultrafast isomerization of retinal within the binding pocket (Polli et al. 2010). Overall, the ^{2}H NMR structure of retinal and its orientation in the binding pocket are in quite good agreement with the crystallographic data (Okada et al. 2004).

Light Activation Yields Relaxation of Torsional Twisting of Retinal Chromophore Bound to Rhodopsin

The above approach has also been used to explore the structural changes of the retinylidene ligand that initiate the large-scale protein conformational changes of the photopigment upon light activation. In the Meta-I state, the allowed solutions for the torsion angles are $\pm 32 \pm 7°$ and $\pm 57 \pm 7°$ for the angle between planes A and B (the β-ionone ring and the polyene chain) and $\pm 173 \pm 4°$ for the angle between planes B and C (Struts et al. 2007). As a result, eight combinations of the angles and the corresponding retinal structures are possible. Insertion of the retinal into the rhodopsin binding pocket in the dark state establishes that most of the eight possible structures have the β-ionone ring position different from the dark state (Struts et al. 2007). Furthermore, electron crystallography data indicate the β-ionone ring does not change its position in the Meta-I state versus the dark state (Ruprecht et al. 2004). Just two of the possible solutions for the ^{2}H NMR retinal structure in the Meta-I state have the β-ionone ring in a position similar to the dark state: one is shown in Fig. 2d with the torsion angles between the planes A–B and B–C of $-32°$ and $+ 173°$, respectively. The other, with corresponding torsion angles of $32 \pm 7°$ and $-173 \pm 4°$, can be obtained from the first structure as a mirror image reflected in a vertical plane (Struts et al. 2007).

A related aspect is that electron crystallography of frozen specimens does not reveal appreciable displacements of the seven transmembrane helices of rhodopsin in the Meta-I state versus the dark state. Hence, the shape of the retinal-binding pocket should be essentially the same. In that case, the second of the above retinal structures seems unlikely, owing to multiple steric clashes within the binding pocket. That leaves us with the

only possible retinal structure in the Meta-I state presented in Fig. 2d. This structure indicates only a single steric clash with the side chain of Trp265. As further described below, the main changes in the retinal conformation in the Meta-I state amount to rotation of the polyene chain adjacent to the C13-methyl group toward the C9-methyl group, straightening and elongation of the polyene chain, and a resulting translation of the β-ionone ring toward helix H5. The displacement of the β-ionone ring, which is also observed by X-ray crystallography and ^{13}C NMR (Nakamichi and Okada 2006; Ahuja et al. 2009a) in different rhodopsin photointermediates, is proposed to play a crucial role in the receptor activation. The rotation of the (proximal) part of the polyene chain containing the C13-methyl group may contribute to destabilization of the ionic lock involving the protonated Schiff base and thus facilitate its deprotonation.

Light-Induced Conformational Changes of Rhodopsin Are Shown by Carbon-13 NMR Spectroscopy

An additional solid-state NMR method that has proved to be salutary for structural studies of membrane proteins is 2D dipolar-assisted rotational resonance (DARR) ^{13}C NMR spectroscopy (Ahuja et al. 2009b; Kimata et al. 2016). This technique enables one to determine close contacts between selectively labeled carbon atoms in the protein. If the mean distance between the labeled atoms is 5 Å or less (Fig. 3a), one can observe a cross-peak in 2D DARR NMR spectra between ^{13}C-labels (Fig. 3b), whereas for larger distances a cross-peak is absent. Such experiments have mapped the distance changes between the labeled carbons of both retinal and the amino acid residues in the binding pocket of metarhodopsin-II (Meta-II) versus the dark state (Fig. 3c–h). Labeled amino acids included tyrosine, serine, cysteine, glycine, threonine, and others. To stabilize the active Meta-II state, rhodopsin was solubilized in detergent micelles and then frozen (1% *n*-dodecyl maltoside solution). Upon light absorption, the DARR NMR spectra revealed displacement of the retinal β-ionone ring within its rhodopsin binding cavity toward helix H5 (Ahuja et al. 2009a; Kimata et al. 2016) accompanied by movement of the E2 loop toward the extracellular side of the membrane (Ahuja et al. 2009b) consistent with ^{2}H NMR data (Brown et al. 2010).

Solid-State Deuterium NMR Relaxation Unveils Functional Dynamics of Retinal Ligand

Application of solid-state NMR relaxation is particularly useful for membrane protein studies, because it gives novel information on local dynamics and intramolecular interactions of biomolecules that is unavailable with other methods (Struts et al. 2011a, b). Dynamics of the methyl groups of the retinal bound to rhodopsin in the dark, Meta-I, and Meta-II states of rhodopsin have been studied by solid-state ^{2}H NMR relaxation. Figure 4 provides a summary of the experimental temperature dependences of the deuterium relaxation times of Zeeman (T_{1Z}) and quadrupolar (T_{1Q}) order for retinal bound to rhodopsin in lipid membranes. Relaxation times T_{1Z} and T_{1Q} are characterized by the spectral densities of the thermal fluctuations of the quadrupolar coupling tensor near the resonance frequency and read:

$$1/T_{1Z} = \frac{3}{4}\pi^2\chi_Q^2[J_1(\omega_0) + 4J_2(2\omega_0)] \qquad (2)$$

$$1/T_{1Q} = \frac{9}{4}\pi^2\chi_Q^2 J_1(\omega_0) \qquad (3)$$

Here χ_Q is the static quadrupolar coupling constant, $J_m(m\omega_0)$ denotes the spectral density

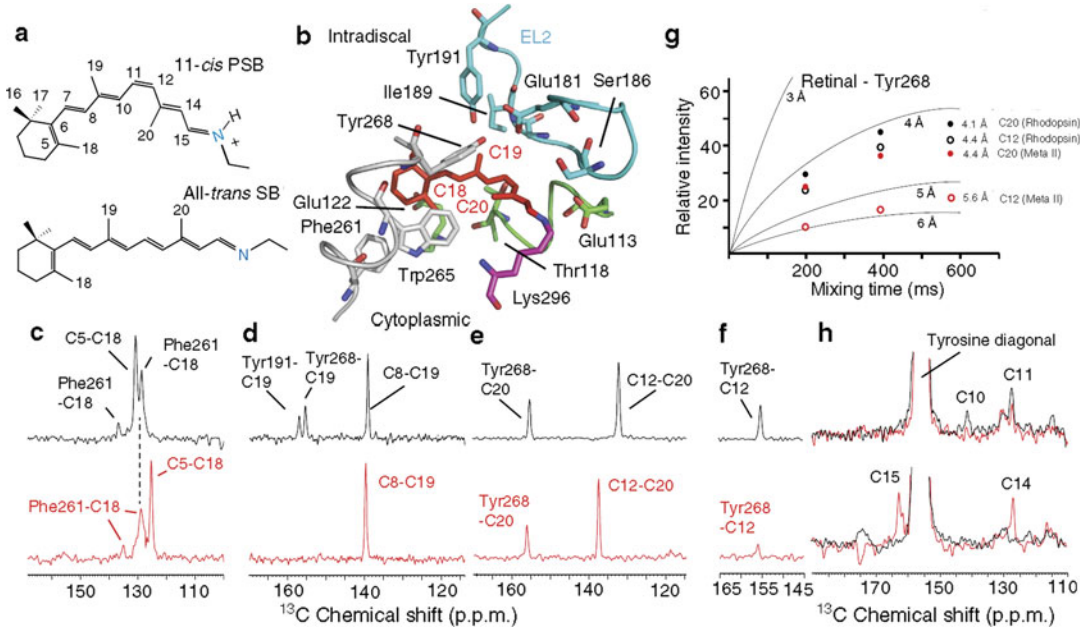

Rhodopsin Activation in Lipid Membranes Based on Solid-State NMR Spectroscopy, Fig. 3 Solid-state ^{13}C NMR evaluates distance restraints that change upon light activation of rhodopsin. (**a**) Structure and numbering scheme of 11-*cis* retinal with protonated Schiff base in the dark state of rhodopsin and all-*trans* retinal with deprotonated Schiff base in the active Meta-II state. (**b**) Crystal structure of retinal-binding pocket of rhodopsin (PDB code: 1U19) (Okada et al. 2004) showing interactions of the retinylidene C18, C19, and C20 carbons with surrounding residues. (**c**–**f**) ^{13}C cross-peak resonances from ^{13}C DARR NMR spectra of rhodopsin (black) and Meta-II (red) obtained for the photoreceptor containing either selectively ^{13}C-labeled retinal and ^{13}C-ring-labeled phenylalanine or selectively ^{13}C-labeled retinal and $^{13}C\zeta$-labeled tyrosine. Cross-peak intensities are inversely related to distances between ^{13}C atoms of retinylidene methyl groups and those of phenylalanine or tyrosine residues. (**g**) Cross-peak resonance intensities at different mixing times compared with buildup curves derived from model compounds showing accuracy of distance measurements between C12 and C20 carbons of the retinal and Tyr268. (**h**) Cross-peaks of $^{13}C\zeta$-Tyr268 with the retinal $^{13}C10,11$ resonances (top) and the $^{13}C14,15$ resonances in rhodopsin (black) and Meta-II (red). (Adapted with permission from Kimata et al. (2016))

($m = 1,2$), and ω_0 is the nuclear resonance (Larmor) frequency.

Now, in terms of generalized model-free analysis (Brown 1982; Struts et al. 2011a), the spectral densities $J_m(m\omega_0)$ are given by:

$$J_m(\omega) = \sum_{r,q} \left| D^{(2)}_{0r}(\Omega_{\mathrm{PI}}) \right|^2 \left[\left\langle \left| D^{(2)}_{rq}(\Omega_{\mathrm{IM}}) \right|^2 \right\rangle - \left| \left\langle D^{(2)}_{rq}(\Omega_{\mathrm{IM}}) \right\rangle \right|^2 \delta_{r0}\delta_{q0} \right] j^{(2)}_{rq}(\omega) \left| D^{(2)}_{qm}(\Omega_{\mathrm{ML}}) \right|^2 \quad (4)$$

where $\omega = m\omega_0$ and $m = 1,2$ (Brown 1982). The quantities in square brackets are the mean-square amplitudes of motion, and the corresponding reduced spectral densities are designated as $j^{(2)}_{rq}(\omega)$. In Eq. (4) $\mathbf{D}^{(j)}(\Omega_{ij})$ denotes the Wigner rotation matrix of rank j (Brown 1996; Molugu et al. 2017), where $\Omega_{ij} \equiv (\alpha_{ij}, \beta_{ij}, \gamma_{ij})$ are the Euler angles describing the relative spatial orientations of coordinate systems i,j = P,I,M,L. Referring back to Fig. 1, the label P means the principal axis system of the electric field gradient (EFG) tensor for an ^2H nucleus (principal z-axis is

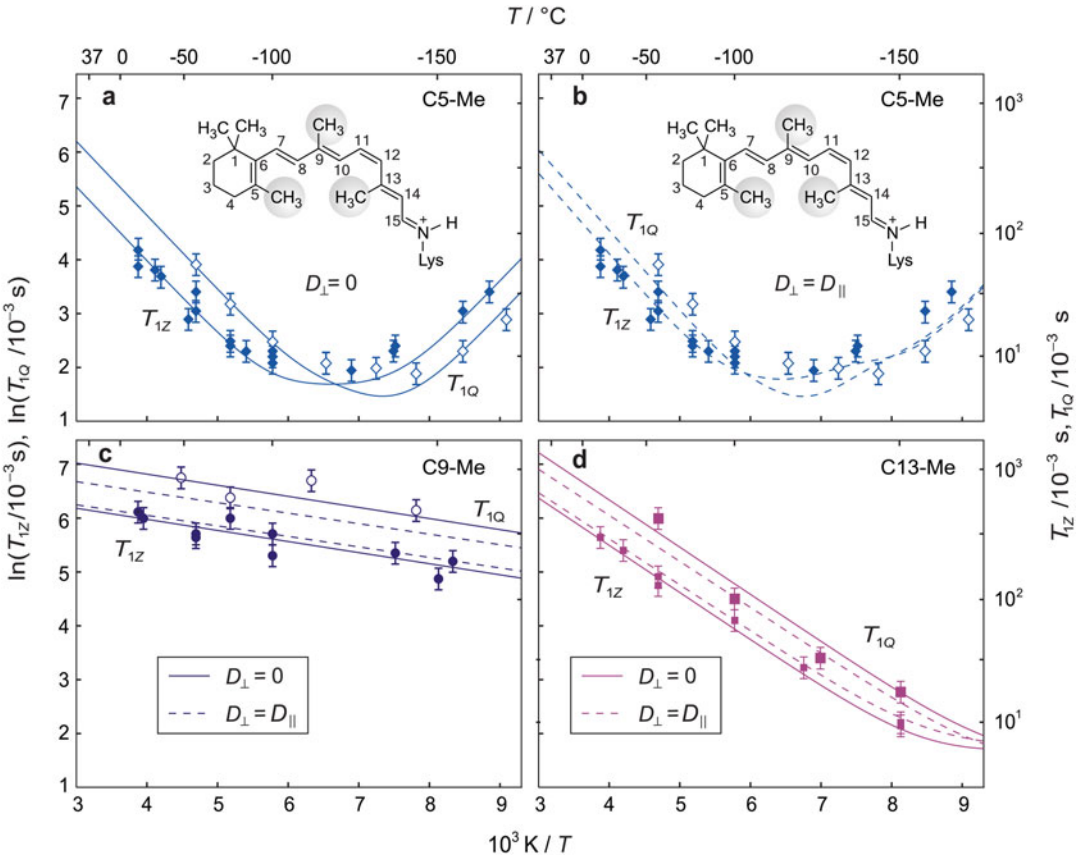

Rhodopsin Activation in Lipid Membranes Based on Solid-State NMR Spectroscopy, Fig. 4 Solid-state ^{2}H NMR relaxation times reveal site-specific differences in the mobility of retinal within the binding cavity of rhodopsin. Spin-lattice (T_{1Z}) and quadrupolar order (T_{1Q}) relaxation times are plotted against inverse temperature for rhodopsin in aligned POPC membranes (1:50 molar ratio) in the dark state with retinal ^{2}H-labeled at (**a**, **b**) the C5-methyl, (**c**) the C9-methyl, or (**d**) the C13-methyl groups. Experimentally determined T_{1Z} and T_{1Q} times were fit simultaneously using analytical models for molecular dynamics (Brown 1982; Xu et al. 2014) (see text): axial threefold jump model (rate constant k, solid lines); continuous rotational diffusion model (coefficients $D_\parallel$ and $D_\perp$ with solid lines for $D_\perp = 0$ and dashed lines for $D_\perp = D_\parallel$). (Adapted with permission from Brown and Struts (2014))

parallel to C–^{2}H bond); I is for an intermediate coordinate frame for the instantaneous methyl orientation (z-axis is C_3 symmetry axis of C–C^{2}H$_3$ bond); M represents the coordinate frame for the average methyl orientation (z-axis is average C–C^{2}H$_3$ bond direction); and L signifies the laboratory frame (z-axis is external magnetic field). For unoriented (powder-type) samples, averaging over all the methyl orientations is carried out (Moltke et al. 1998). Assuming exponential relaxation, the reduced spectral densities are given by $j_{rq}^{(2)}(\omega) = 2\tau_{rq}/\left(1+\omega^2{\tau_{rq}}^2\right)$ where τ_{rq} are the (rotational) correlation times for the individual Wigner rotation matrix elements.

Further data analysis and reduction then introduce a motional model to describe the molecular fluctuations (Brown 1982). As one example, for the case of N-fold hops about a single axis, the correlation times read (Brown 1982; Torchia and Szabo 1982) $1/\tau_{rq} \rightarrow 1/\tau_r = 4k\sin^2(\pi r/N)$ (axial averaging is assumed) which yields $1/\tau_r = 3k$ for a methyl group. Alternatively, for continuous diffusion in a potential of mean force (Trouard et al. 1994), the rotational correlation times read (Brown 1982):

$$\frac{1}{\tau_{rq}} = \frac{\mu_{rq}}{\left\langle \left| D_{rq}^{(2)}(\Omega_{\mathrm{IM}}) \right|^2 \right\rangle - \left| \left\langle D_{rq}^{(2)}(\Omega_{\mathrm{IM}}) \right\rangle \right|^2 \delta_{r0}\delta_{q0}} D_{\perp} + \left(D_{\parallel} - D_{\perp}\right) r^2 \quad (5)$$

In the above expression, the diffusion coefficients $D_{\parallel}$ and $D_{\perp}$ quantify axial and off-axial rotations of a methyl group. The moments μ_{rq} and the mean-squared moduli $\langle |D_{rq}^{(2)}(\Omega_{\mathrm{IM}})|^2 \rangle$ depend on the second- and fourth-rank order parameters (Trouard et al. 1994). In a strong-collision approximation, the orientation changes by any amount, and the correlation times are those of a rigid rotor (Brown 1982): $1/\tau_{rq} \rightarrow 1/\tau_r = 6D_{\perp} + (D_{\parallel} - D_{\perp})r^2$.

For either a threefold jump or continuous diffusion model, the rotational correlation times are inversely related to $A \exp(-E_a/RT)$, where A is the preexponential factor (k_0 or D_0) and E_a is the activation energy (barrier) for the methyl rotation (Struts et al. 2011a). Both models have been used to fit experimental relaxation data for rhodopsin (Struts et al. 2011a). In the dark, Meta-I, and Meta-II states, the temperature dependences of the T_{1Z} relaxation times can be fit using either the jump or continuous diffusion models. Measurement of both Zeeman and quadrupolar order relaxation allows one to obtain additional information on anisotropy of the local molecular motions (Struts et al. 2011a).

Dynamical Hot Spots of Bound Retinal Are Affected by Light-Induced Isomerization

By application of the above experimental approach, for rhodopsin in the dark state, rotational correlation times are found in the range of 2–12 ps at 30 °C and 3–45 ps at −60 °C, depending on the methyl group. The T_{1Z} and T_{1Q} temperature dependences manifest the activation energy for the methyl dynamics, and are related to the height of the rotational potential barriers (Fig. 4). Although surprising, the low activation energy for the C9-methyl group can be explained by compensation of the intra-retinal 1–6 interactions with hydrogens H7 and H11 (Fig. 4a), because the corresponding rotational potentials are offset versus one another by about 60°. Higher activation energies for the C5- and C13-methyl groups are the result of intra-retinal 1–7 interactions with the H8 and H10 hydrogens, respectively. What is more, the high activation energy for the C5-methyl group indicates a 6-*s*-*cis* conformation of the β-ionone ring. Contributions due to interactions with the amino acid side chains of the binding pocket of rhodopsin are smaller, owing to the larger distances from the methyl groups (>4 Å) (Fig. 4).

Site-Specific Changes in Retinal Dynamics Underlie Light Activation of Rhodopsin

A further significant aspect is that changes in the dynamics of the retinal methyl groups are clearly evident in the Meta-I and the Meta-II states after photoisomerization (Fig. 5) (Struts et al. 2011a). The Meta-I and Meta-II states of rhodopsin were quantitatively cryotrapped in POPC and POPC: DOPE (3:1 ratio) bilayers, respectively (Struts et al. 2011a). The largest photoinduced changes occur for the C9-methyl group, whose activation energy E_a increases progressively from the dark to the Meta-I state and then to Meta-II. At the same time, the E_a value for the C13-methyl group decreases progressively going from the Meta-I to the Meta-II states. It follows that upon isomerization to yield *trans* retinal, the activation energies and spin-lattice relaxation times become comparable for both the C13- and C9-methyl groups (Fig. 5), which seems logical because both groups are now on the same side of the molecule, with similar rotational barriers (Fig. 2d). The diminution of the activation energy for the C13-methyl group can be explained analogously to the low E_a value for the C9-methyl group in the dark state, viz., by compensation of intra-retinal 1–6 interactions with hydrogens H11 and H15, whose rotational potentials are in antiphase (60° phase shift; see above). The greater activation energy for the C9-methyl group and decrease in mobility upon retinal isomerization can be explained by changes in the retinal conformation and possible

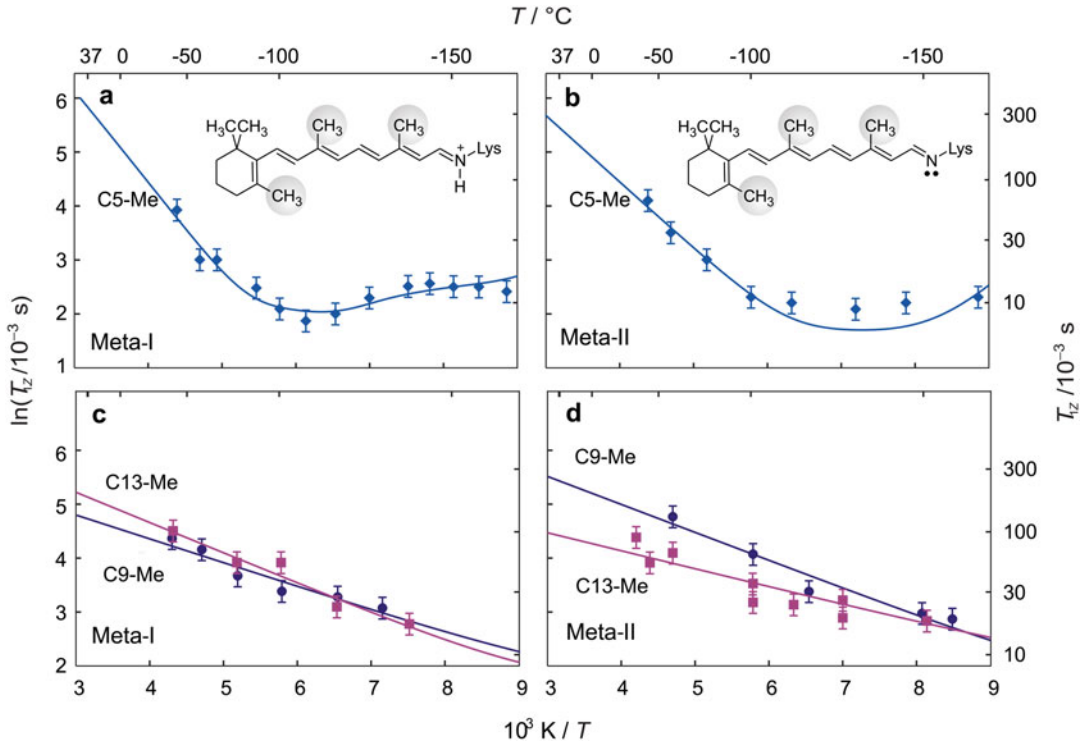

Rhodopsin Activation in Lipid Membranes Based on Solid-State NMR Spectroscopy, Fig. 5 Deuterium NMR relaxation establishes changes in dynamics of the retinylidene methyl groups upon light activation of rhodopsin. Spin-lattice relaxation times (T_{1Z}) are graphed against inverse temperature for rhodopsin in POPC membranes (1:50 molar ratio) with retinal ^{2}H-labeled at the C5-, C9-, or C13-methyl groups, respectively, in (**a**, **c**) the Meta-I and (**b**, **d**) the Meta-II states. The relaxation data are fit with both an axial threefold jump model (rate constant k) and a diffusion model (axial coefficient $D_{\|}$ with $D_{\perp} = 0$). For the C5-methyl group in Meta-I either different rotational diffusion constants were assumed ($D_{\|} \neq D_{\perp}$, not shown) or different conformers (Struts et al. 2011b). Following 11-*cis* to *trans* isomerization, a reduction occurs from three distinct methyl environments in the dark state to ~ two environments in Meta-I and Meta-II indicating a more planar retinal conformation. (Adapted with permission from Brown and Struts (2014))

interactions with the surrounding amino acid side chains (e.g., Tyr268 or Thr118) in the binding pocket. Notably, the observed E_a barriers do not indicate any steric clashes of the C9-methyl and the C13-methyl groups in the Meta-I and Meta-II states. For the C5-methyl group, some interesting and unusual changes are observed in the T_{1Z} temperature dependence in the Meta-I state (Struts et al. 2011a). But overall, the activation energy for C5-methyl rotation does not change much in the transition from the dark to the active Meta-II state. As a result, one can conclude that the conformation and the environment of the β-ionone ring remain similar after rhodopsin activation (Struts et al. 2011a).

Understanding Rhodopsin Activation Requires X-Ray Diffraction and Magnetic Resonance Approaches

According to current understanding, rhodopsin activation is the outcome of retinal conformational changes that disrupt a system of hydrogen-bonding networks and electrostatic interactions that stabilize the inactive state, first unlocking the receptor around the retinal, and then in more distal domains. Release of the constraints transforms the receptor into its intrinsic active state, which has been proposed to resemble the ligand-free opsin structure, with the formation of new hydrogen-bonding networks. Conversion of the

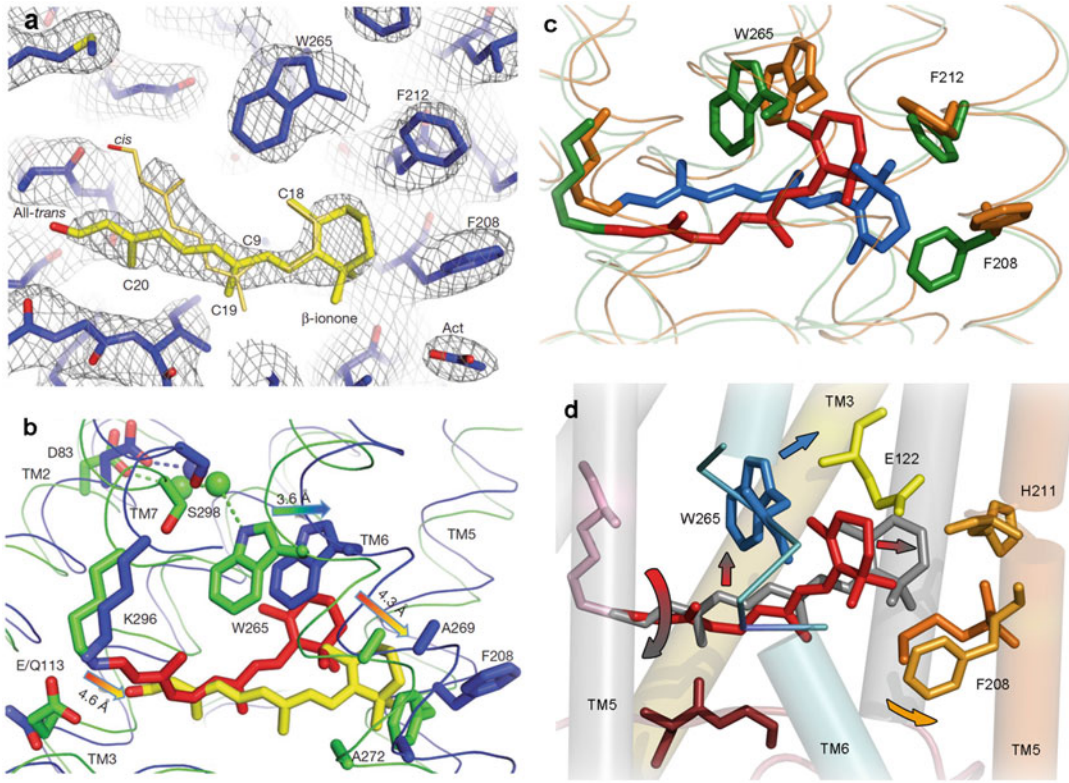

Rhodopsin Activation in Lipid Membranes Based on Solid-State NMR Spectroscopy, Fig. 6 Local changes in retinal initiate large-scale protein rearrangements leading to receptor activation. (**a**) Electron density map and (**b**) PDB structure (2X72, blue) of constitutively active rhodopsin mutant Glu113Gln with the bound GαCT peptide (Standfuss et al. 2011) versus rhodopsin structure in dark state (PDB code: 1GZM, green). Note that all-*trans* retinal (yellow) is not covalently bound to Lys296. (Adapted with permission from Standfuss et al. (2011)). (**c**) Retinal conformation in the Meta-II state (PDB code: 3PQR, blue; protein is shown in orange) compared with the dark state (PDB code: 1U19, red; protein is green) (Okada et al. 2004; Choe et al. 2011). (**d**) Data from solid-state ^{2}H NMR spectroscopy (Struts et al. 2011a) and other biophysical measurements suggest the C13-methyl and the C=NH^{+}– groups of the protonated Schiff base change their orientation upon ligand isomerization. Note that the *β*-ionone ring with its C5-methyl group remains in its hydrophobic pocket, but its displacement due to elongation of retinal triggers allosteric movements of helices H5 and H6 that lead to rhodopsin activation (see text). (Figure produced with/using PyMOL (http://pymol.sourceforge.net/))

photonic energy into thermal motions that include helical fluctuations enables transitions over the barriers that separate the inactive, preactive, and active states. Still, a detailed picture of the activation mechanism is more complicated, which is not completely understood at present (Patel et al. 2004; Vogel et al. 2005; Nakamichi and Okada 2006; Struts et al. 2007, 2011a; Altenbach et al. 2008; Mahalingam et al. 2008; Ahuja et al. 2009b; Choe et al. 2011; Standfuss et al. 2011; Kimata et al. 2016). Figure 6 illustrates the changes in the retinal-binding pocket that occur in the activation process. In Fig. 6a an electron density map is depicted for the constitutively active rhodopsin mutant E113Q in complex with a peptide derived from the carboxyl terminus of the α-subunit of the G-protein transducin (GαCT peptide) (Standfuss et al. 2011). Figure 6b shows the 3D structure of the constitutive E113Q mutant (PDB code: 2X72) superimposed with ground-state rhodopsin (PDB code: 1GZM). However, a different retinal conformation has been observed for opsin regenerated with all-*trans* retinal to form the putative active Meta-II state (Choe et al. 2011).

Superposition of this retinal structure (PDB code: 3PQR) with the ligand conformation in rhodopsin (PDB code: 1U19) (Okada et al. 2004) is provided in Fig. 6c. Additionally Fig. 6d shows the ^{2}H NMR structure of retinal in the Meta-I state overlapped with the binding pocket of rhodopsin in the dark state (Struts et al. 2007, 2011b). A relaxed all-*trans* conformation of ligand and displacement of its β-ionone ring are clearly evident in the Meta-I (Fig. 6d) and the Meta-II (Fig. 6b, c) states.

Data for the ^{2}H NMR retinal structure and dynamics in different states can then be combined with other structural and biophysical studies (Fujimoto et al. 2002; Patel et al. 2004; Vogel et al. 2005; Nakamichi and Okada 2006; Mahalingam et al. 2008; Altenbach et al. 2008; Ahuja et al. 2009a; Choe et al. 2011; Standfuss et al. 2011; Kimata et al. 2016), leading to the following mechanism of rhodopsin activation (Struts et al. 2011b). Photoisomerization of retinal gives a rotation of the C13-methyl group and the adjacent part of the retinal polyene chain toward the β4-sheet on the extracellular loop E2 (Nakamichi and Okada 2006; Struts et al. 2007). Notably, the polyene chain of the retinal straightens and elongates significantly (Struts et al. 2007; Choe et al. 2011). Straightening of the polyene chain leads to displacement of the β-ionone ring toward helix H5. Rotation of the retinal polyene chain, with the C13-methyl group attached at the Schiff base end of the ligand, destabilizes the H-bonding networks connecting the E2 loop; helices H1–H3, H6, and H7; and retinal in the inactive state (this includes the ionic lock between the protonated Schiff base and its counterion Glu113) (Okada et al. 2004; Vogel et al. 2004; Martínez-Mayorga et al. 2006). What is more, the ionic lock of the protonated Schiff base with its (complex) counterion may be destabilized by the 11-*cis* to *trans* retinal isomerization, which changes the pK_A of the protonated Schiff base (Mahalingam et al. 2008; Mertz et al. 2011; Zhu et al. 2013). Rearrangement of the H-bonding network (Choe et al. 2011) and deprotonation of the Schiff base break the ionic lock, thus enabling rearrangement of the helical bundle. Displacement of the β-ionone ring (whose C5-methyl group is in the vicinity of Glu122 in the dark state) toward helix H5 may contribute to rearrangement of another H-bonding network between Glu122 on H3 and His211 on H5 (Vogel et al. 2005; Struts et al. 2007; Choe et al. 2011), which initially stabilizes the inactive conformation. It appears to be also coupled to rotation of the cytoplasmic end of helix H5 closer to H6 (Ahuja et al. 2009a). Because of this motion, the ionic lock between the helices H3 and H6 involving Glu134, Arg135, and Glu247 is destabilized. Consequently, the activating rotation of the helix H6 occurs accompanied by transient opening of the transducin-binding site (Scheerer et al. 2008; Struts et al. 2011a, b).

Multiscale Protein Dynamics Explain Rhodopsin Function in Lipid Membranes

To recapitulate at this point, in the sequence of the events in rhodopsin activation, the early photointermediates (photo-, batho-, lumirhodopsin) are followed by the major reactions: Meta-I $\rightleftharpoons$ Meta-II$_a$ $\rightleftharpoons$ Meta-II$_b$ + H_3O^+ $\rightleftharpoons$ Meta-II$_b$H$^+$, where Meta-II$_b$ and Meta-II$_b$H$^+$ are active conformational substates (Mahalingam et al. 2008; Zaitseva et al. 2010; Struts et al. 2015a, b). All of the substates (from Meta-I to Meta-II$_b$H$^+$) are in thermodynamic equilibrium after decay of the preceding lumirhodopsin state in the activation. The above picture of rhodopsin activation naturally raises the question: are these the only substates of rhodopsin in the activation process? An important aspect is how the local isomerization of retinal (Struts et al. 2007) initiates the large-scale helix fluctuations in the Meta-I to Meta-II equilibrium (Struts et al. 2011b). In the dark state, the induced fit of retinal to the binding pocket enforces a highly twisted conformation upon the ligand (Struts et al. 2007). Our molecular dynamics (MD) simulations clearly indicate that in the dark state not only the cytoplasmic loops but also the extracellular loops of rhodopsin undergo μs-ms timescale motions. Even so, the transmembrane (TM) helical core is more stable (Huber et al. 2004; Leioatts et al. 2014). Large-scale functional protein motions – such as the Meta-I to Meta-II fluctuations of rhodopsin – have large

activation barriers that still can be overcome by thermal motion. They occur infrequently due to their collective nature, because they involve displacements of many atoms within the protein core on the millisecond timescale.

Rhodopsin has been proposed to be partially unfolded in the Meta-II state (Brown 1994), and so an ensemble of conformers is to be expected (Mahalingam et al. 2008; Zaitseva et al. 2010). Based on the above activation mechanism, it follows that allosteric interactions trigger concerted movements of the TM helices, together with changes in the cytoplasmic loops that expose the transducin (G_t) recognition sites. Extension of helix H5 (Park et al. 2008) and a rigid-body rotation of H6 as first shown by Hubbell et al. (Altenbach et al. 2008) lead to an overall elongation of the protein (Botelho et al. 2006), accompanied by its expansion within the lipid bilayer (Attwood and Gutfreund 1980). Starting from a highly locked receptor core with extremely low basal activity, activation of rhodopsin generates an opening of the protein, whereby the collective, large-scale protein fluctuations are accompanied by a gain in partial molar volume (Attwood and Gutfreund 1980). A concomitant loosening of the receptor core enables increased water penetration to the ligand-binding cavity (Perera et al. 2016). These conclusions differ from the conventional view of a single light-activated receptor (R^*) conformation. Even so, the notion of a dynamically activated receptor (DAR) explains how the large-scale protein fluctuations in rhodopsin activation are initiated by the local retinal dynamics.

What is more, the presence of multiple active substates in the Meta-I to Meta-II equilibrium (Struts et al. 2011b) may explain the different orientations of the retinal in the Meta-II state reported by different groups (Patel et al. 2004; Ahuja et al. 2009a; Choe et al. 2011; Standfuss et al. 2011; Deupi et al. 2012; Kimata et al. 2016). In the X-ray structures of Meta-II, obtained either by soaking native opsin crystals with all-*trans* retinal or for the constitutive M257Y/D282C rhodopsin double mutant, the retinal is rotated by ~ 90–180° about its long axis as compared to rhodopsin in the dark state (Fig. 6c) (Choe et al. 2011; Deupi et al. 2012). Yet the distance constraints obtained from dipolar-assisted rotational resonance NMR spectroscopy for Meta-II in detergent suspensions (Patel et al. 2004; Ahuja et al. 2009a; Kimata et al. 2016) indicate an opposite orientation of the retinal ligand, which is supported by the X-ray crystal structure of the active E113Q rhodopsin mutant (Standfuss et al. 2011). In studying rhodopsin activation, the influences of the environment must clearly be taken into account. For example, at high pH and low temperature (Mahalingam et al. 2008) or with dehydrating conditions (Salinas et al. 2018), rhodopsin activation does not proceed beyond the Meta-I state. Furthermore, under physiological conditions the receptor conformation in the Meta-II state may change more than predicted by X-ray crystallography, as suggested by time-resolved wide-angle X-ray scattering (TR-WAXS) experiments (Malmerberg et al. 2015). Differences in environment conditions may thus provide an alternate explanation for the different retinal orientations observed in the various experiments. Although substantial further work is needed to firmly establish the nature of the activated state(s) of rhodopsin, it is clear that solid-state NMR spectroscopy can probe the various tiers of the protein energy landscape (Shrestha et al. 2016; Perera et al. 2018). Solid-state NMR has an important role to play in combination with X-ray diffraction, because it is exquisitely sensitive to dynamics (Struts et al. 2007; Xu et al. 2014). The implementation of innovative new crystallography and magnetic resonance approaches can be expected to contribute to a fuller understanding of the structure and functioning of rhodopsin and other membrane proteins. These subjects are certain to occupy membrane biophysicists for years to come.

Conclusions and Future Outlook

Visual rhodopsin is an important model for the largest family of G-protein-coupled receptors, which initiate signal transduction across cellular membranes and are of great pharmaceutical significance. Yet many details of the activation mechanism remain unknown or even

contradictory; for instance, the conformation and orientation of the bound retinal in the active Meta-II state. Solid-state NMR spectroscopy allows investigation of the local structure and molecular motion of the retinal ligand in different rhodopsin intermediates, and moreover illuminates the functional protein dynamics. To characterize light-induced changes in structure and mobility of rhodopsin, site-specific ^{2}H and ^{13}C labels are introduced into the retinal ligand. Solid-state NMR spectra and ^{2}H NMR relaxation times (spin-lattice, T_{1Z}, and quadrupolar order, T_{1Q}) in the dark, Meta-I, and Meta-II states of rhodopsin are acquired by cryotrapping the various states in membrane lipid bilayers. The solid-state NMR data together with results of Fourier transform infrared (FTIR) and site-directed spin spin-labeling (SDSL) spectroscopy show how local changes in the retinal structure trigger activating helical fluctuations of the receptor. Exploring how the Meta-I to Meta-II equilibrium of rhodopsin entails a complex energy landscape – with multiple substates rather than a simple activation switch – is of great importance for biological signaling, in which solid-state NMR spectroscopy can contribute significantly.

Acknowledgments This research was supported by the U.S. National Institutes of Health (EY012049 and EY026041) and by the U.S. National Science Foundation (MCB 1817862 and CHE 1904125).

References

Ahuja S, Crocker E, Eilers M, Hornak V, Hirshfeld A, Ziliox M, Syrett N, Reeves PJ, Khorana HG, Sheves M, Smith SO (2009a) Location of the retinal chromophore in the activated state of rhodopsin. J Biol Chem 284:10190–10201

Ahuja S, Hornak V, Yan ECY, Syrett N, Goncalves JA, Hirshfeld A, Ziliox M, Sakmar TP, Sheves M, Reeves PJ, Smith SO, Eilers M (2009b) Helix movement is coupled to displacement of the second extracellular loop in rhodopsin activation. Nat Struct Mol Biol 16:168–175

Altenbach C, Kusnetzow AK, Ernst OP, Hofmann KP, Hubbell WL (2008) High-resolution distance mapping in rhodopsin reveals the pattern of helix movement due to activation. Proc Natl Acad Sci U S A 105:7439–7444

Attwood PV, Gutfreund H (1980) The application of pressure relaxation to the study of the equilibrium between metarhodopsin I and II from bovine retinas. FEBS Lett 119:323–326

Botelho AV, Huber T, Sakmar TP, Brown MF (2006) Curvature and hydrophobic forces drive oligomerization and modulate activity of rhodopsin in membranes. Biophys J 91:4464–4477

Brown MF (1982) Theory of spin-lattice relaxation in lipid bilayers and biological membranes. ^{2}H and ^{14}N quadrupolar relaxation. J Chem Phys 77:1576–1599

Brown MF (1994) Modulation of rhodopsin function by properties of the membrane bilayer. Chem Phys Lipids 73:159–180

Brown MF (1996) Membrane structure and dynamics studied with NMR spectroscopy. In: Merz KM Jr, Roux B (eds) Biological membranes: a molecular perspective from computation and experiment. Birkhäuser, Basel, pp 175–252

Brown MF, Struts AV (2014) Structural dynamics of retinal in rhodopsin activation viewed by solid-state ^{2}H NMR spectroscopy. In: Separovic F, Naito A (eds) Advances in biological solid-state NMR: proteins and membrane-active peptides. The Royal Society of Chemistry, Cambridge, pp 320–352

Brown MF, Heyn MP, Job C, Kim S, Moltke S, Nakanishi K, Nevzorov AA, Struts AV, Salgado GFJ, Wallat I (2007) Solid-state ^{2}H NMR spectroscopy of retinal proteins in aligned membranes. Biochim Biophys Acta 1768:2979–3000

Brown MF, Salgado GFJ, Struts AV (2010) Retinal dynamics during light activation of rhodopsin revealed by solid-state NMR spectroscopy. Biochim Biophys Acta 1798:177–193

Cavanaugh J, Fairbrother WJ, Palmer AG III, Skelton NJ, Rance M (2006) Protein NMR spectroscopy: principles and practice. Academic, New York

Choe H-W, Kim YJ, Park JH, Morizumi T, Pai EF, Krauβ N, Hofmann KP, Scheerer P, Ernst OP (2011) Crystal structure of metarhodopsin II. Nature 471:651–656

Deupi X, Edwards P, Singhal A, Nickle B, Oprian D, Schertler G, Standfuss J (2012) Stabilized G protein binding site in the structure of constitutively active metarhodopsin-II. Proc Natl Acad Sci U S A 109:119–124

Fujimoto Y, Fishkin N, Pescitelli G, Decatur J, Berova N, Nakanishi K (2002) Solution and biologically relevant conformations of enantiomeric 11-*cis*-locked cyclopropyl retinals. J Am Chem Soc 124:7294–7302

Hu Y, Kienlen-Campard P, Tang T-C, Perrin F, Opsomer R, Decock M, Pan X, Octave J-N, Constantinescu SN, Smith SO (2017) β-Sheet structure within the extracellular domain of C99 regulates amyloidogenic processing. Sci Rep 7:17159

Huber T, Botelho AV, Beyer K, Brown MF (2004) Membrane model for the GPCR prototype rhodopsin: hydrophobic interface and dynamical structure. Biophys J 86:2078–2100

Jäger S, Lewis JW, Zvyaga TA, Szundi I, Sakmar TP, Kliger DS (1997) Chromophore structural changes in

rhodopsin from nanoseconds to microseconds following pigment photolysis. Proc Natl Acad Sci U S A 94:8557–8562

Kimata N, Pope A, Eilers M, Opefi CA, Ziliox M, Hirshfeld A, Zaitseva E, Vogel R, Sheves M, Reeves PJ, Smith SO (2016) Retinal orientation and interactions in rhodopsin reveal a two-stage trigger mechanism for activation. Nat Commun 7:12683

Koehl A, Hu H, Maeda S, Zhang Y, Qu Q, Paggi JM, Latorraca NR, Hilger D, Dawson R, Matile H, Schertler GFX, Granier S, Weis WI, Dror RO, Manglik A, Skiniotis G, Kobilka BK (2018) Structure of the μ-opioid receptor–G_i protein complex. Nature 558:547–552

Latorraca NR, Venkatakrishnan AJ, Dror RO (2017) GPCR dynamics: structures in motion. Chem Rev 117:139–155

Leioatts N, Mertz B, Martínez-Mayorga K, Romo TD, Pitman MC, Feller SE, Grossfield A, Brown MF (2014) Retinal ligand mobility explains internal hydration and reconciles active rhodopsin structures. Biochemistry 53:376–385

Mahalingam M, Martínez-Mayorga K, Brown MF, Vogel R (2008) Two protonation switches control rhodopsin activation in membranes. Proc Natl Acad Sci U S A 105:17795–17800

Malmerberg E, Bovee-Geurts PHM, Katona G, Deupi X, Arnlund D, Wickstrand C, Johansson LC, Westenhoff S, Nazarenko E, Schertler GFX, Menzel A, de Grip WJ, Neutze R (2015) Conformational activation of visual rhodopsin in native disc membranes. Sci Signal 8:ra26

Martínez-Mayorga K, Pitman MC, Grossfield A, Feller SE, Brown MF (2006) Retinal counterion switch mechanism in vision evaluated by molecular simulations. J Am Chem Soc 128:16502–16503

Masureel M, Zou Y, Picard L-P, van der Westhuizen E, Mahoney JP, Rodrigues JPGLM, Mildorf TJ, Dror RO, Shaw DE, Bouvier M, Pardon E, Steyaert J, Sunahara RK, Weis WI, Zhang C, Kobilka BK (2018) Structural insights into binding specificity, efficacy and bias of a β_2AR partial agonist. Nat Chem Biol 14:1059–1066

Mertz B, Lu M, Brown MF, Feller SE (2011) Steric and electronic influences on the torsional energy landscape of retinal. Biophys J 101:L17–L19

Moltke S, Nevzorov AA, Sakai N, Wallat I, Job C, Nakanishi K, Heyn MP, Brown MF (1998) Chromophore orientation in bacteriorhodopsin determined from the angular dependence of deuterium NMR spectra of oriented purple membranes. Biochemistry 37:11821–11835

Molugu TR, Lee S, Brown MF (2017) Concepts and methods of solid-state NMR spectroscopy applied to biomembranes. Chem Rev 117:12087–12132

Nakamichi H, Okada T (2006) Local peptide movement in the photoreaction intermediate of rhodopsin. Proc Natl Acad Sci U S A 103:12729–12734

Nevzorov AA, Moltke S, Heyn MP, Brown MF (1999) Solid-state NMR line shapes of uniaxially oriented immobile systems. J Am Chem Soc 121:7636–7643

Nygaard R, Zou Y, Dror RO, Mildorf TJ, Arlow DH, Manglik A, Pan AC, Liu CW, Fung JJ, Bokoch MP, Thian FS, Kobilka TS, Shaw DE, Mueller L, Prosser RS, Kobilka BK (2013) The dynamic process of β_2-adrenergic receptor activation. Cell 152:532–542

Okada T, Sugihara M, Bondar A-N, Elstner M, Entel P, Buss V (2004) The retinal conformation and its environment in rhodopsin in light of a new 2.2 Å crystal structure. J Mol Biol 342:571–583

Park JH, Scheerer P, Hofmann KP, Choe H-W, Ernst OP (2008) Crystal structure of the ligand-free G-protein-coupled receptor opsin. Nature 454:183–187

Patel AB, Crocker E, Eilers M, Hirshfeld A, Sheves M, Smith SO (2004) Coupling of retinal isomerization to the activation of rhodopsin. Proc Natl Acad Sci U S A 101:10048–10053

Perera SMDC, Chawla U, Brown MF (2016) Powdered G-protein-coupled receptors. J Phys Chem Lett 7:4230–4235

Perera SMDC, Xu X, Struts AV, Chawla U, Boutet S, Carbajo S, Seaberg MD, Hunter MS, Martin-Garcia JM, Coe JD, Wiedorn MO, Nelson G, Chamberlain S, Deponte DP, Fromme R, Grant TD, Kirian RA, Fromme P, Brown MF (2017) Time-resolved wide-angle X-ray scattering reveals protein quake in rhodopsin activation. Biophys J 112:506a–507a

Perera SMDC, Chawla U, Shrestha UR, Bhowmik D, Struts AV, Qian S, Chu X-Q, Brown MF (2018) Small-angle neutron scattering reveals energy landscape for rhodopsin photoactivation. J Phys Chem Lett 9:7064–7071

Polli D, Altoe P, Weingart O, Spillane KM, Manzoni C, Brida D, Tomasello G, Orlandi G, Kukura P, Mathies RA, Garavelli M, Cerullo G (2010) Conical intersection dynamics of the primary photoisomerization event in vision. Nature 467:440–443

Ruprecht JJ, Mielke T, Vogel R, Villa C, Schertler GFX (2004) Electron crystallography reveals the structure of metarhodopsin I. EMBO J 23:3609–3620

Salgado GFJ, Struts AV, Tanaka K, Fujioka N, Nakanishi K, Brown MF (2004) Deuterium NMR structure of retinal in the ground state of rhodopsin. Biochemistry 43:12819–12828

Salinas AM, Perera SMDC, Brown MF (2018) Hydration thermodynamics of a powdered G-protein-coupled receptor. Biophys J 114:240a

Salom D, Lodowski DT, Stenkamp RE, Trong IL, Golczak M, Jastrzebska B, Harris T, Ballesteros JA, Palczewski K (2006) Crystal structure of a photoactivated deprotonated intermediate of rhodopsin. Proc Natl Acad Sci U S A 103:16123–16128

Scheerer P, Park JH, Hildebrand PW, Kim YJ, Krauβ N, Choe H-W, Hofmann KP, Ernst OP (2008) Crystal structure of opsin in its G-protein-interacting conformation. Nature 455:497–502

Shrestha UR, Perera SMDC, Bhowmik D, Chawla U, Mamontov E, Brown MF, Chu X-Q (2016) Quasi-

elastic neutron scattering reveals ligand-induced protein dynamics of a G-protein-coupled receptor. J Phys Chem Lett 7:4130–4136

Spooner PJR, Sharples JM, Verhoeven MA, Lugtenberg J, Glaubitz C, Watts A (2002) Relative orientation between the β-ionone ring and the polyene chain for the chromophore of rhodopsin in native membranes. Biochemistry 41:7549–7555

Spooner PJR, Sharples JM, Goodall SC, Seedorf H, Verhoeven MA, Lugtenburg J, Bovee-Geurts PHM, DeGrip WJ, Watts A (2003) Conformational similarities in the β-ionone ring region of the rhodopsin chromophore in its ground state and after photoactivation to the metarhodopsin-I intermediate. Biochemistry 42:13371–13378

Standfuss J, Edwards PC, D'Antona A, Fransen M, Xie G, Oprian DD, Schertler GFX (2011) The structural basis of agonist-induced activation in constitutively active rhodopsin. Nature 471:656–660

Stevens RC, Cherezov V, Katritch V, Abagyan R, Kuhn P, Rosen H, Wüthrich K (2013) The GPCR network: a large-scale collaboration to determine human GPCR structure and function. Nat Rev Drug Discov 12:25–34

Struts AV, Salgado GFJ, Tanaka K, Krane S, Nakanishi K, Brown MF (2007) Structural analysis and dynamics of retinal chromophore in dark and Meta I states of rhodopsin from ^{2}H NMR of aligned membranes. J Mol Biol 372:50–66

Struts AV, Salgado GFJ, Brown MF (2011a) Solid-state ^{2}H NMR relaxation illuminates functional dynamics of retinal cofactor in membrane activation of rhodopsin. Proc Natl Acad Sci U S A 108:8263–8268

Struts AV, Salgado GFJ, Martínez-Mayorga K, Brown MF (2011b) Retinal dynamics underlie its switch from inverse agonist to agonist during rhodopsin activation. Nat Struct Mol Biol 18:392–394

Struts AV, Barmasov AV, Brown MF (2015a) Spectral methods for study of the G-protein-coupled receptor rhodopsin: I. vibrational and electronic spectroscopy. Opt Spectrosc 118:711–717

Struts AV, Chawla U, Perera SMDC, Brown MF (2015b) Investigation of rhodopsin dynamics in its signaling state by solid-state deuterium NMR spectroscopy. Methods Mol Biol 1271:133–158

Struts AV, Barmasov AV, Brown MF (2016) Spectral methods for study of the G-protein-coupled receptor rhodopsin: II. Magnetic resonance methods. Opt Spectrosc 120:286–293

Torchia DA, Szabo A (1982) Spin-lattice relaxation in solids. J Magn Reson 49:107–121

Trouard TP, Alam TM, Brown MF (1994) Angular dependence of deuterium spin-lattice relaxation rates of macroscopically oriented dilaurylphosphatidylcholine in the liquid-crystalline state. J Chem Phys 101:5229–5261

Van Eps N, Preininger AM, Alexander N, Kaya AI, Meier S, Meiler J, Hamm HE, Hubbell WL (2011) Interaction of a G protein with an activated receptor opens the interdomain interface in the alpha subunit. Proc Natl Acad Sci U S A 108:9420–9424

Verdegem PJE, Bovee-Geurts PHM, de Grip WJ, Lugtenburg J, de Groot HJM (1999) Retinylidene ligand structure in bovine rhodopsin, metarhodopsin-I, and 10-methylrhodopsin from internuclear distance measurements using ^{13}C-labeling and 1-D rotational resonance MAS NMR. Biochemistry 38:11316–11324

Vogel R, Ruprecht J, Villa C, Mielke T, Schertler GFX, Siebert F (2004) Rhodopsin photoproducts in 2D crystals. J Mol Biol 338:597–609

Vogel R, Siebert F, Lüdeke S, Hirshfeld A, Sheves M (2005) Agonists and partial agonists of rhodopsin: retinals with ring modifications. Biochemistry 44:11684–11699

Wu W, Nogly P, Rheinberger J, Kick LM, Gati C, Nelson G, Deupi X, Standfuss J, Schertler G, Panneels V (2015) Batch crystallization of rhodopsin for structural dynamics using an X-ray free-electron laser. Acta Crystallogr F71:856–860

Xu X, Struts AV, Brown MF (2014) Generalized model-free analysis of nuclear spin relaxation experiments. eMag Res 3:275–286

Zaitseva E, Brown MF, Vogel R (2010) Sequential rearrangement of interhelical networks upon rhodopsin activation in membranes: the Meta II_a conformational substate. J Am Chem Soc 132:4815–4821

Zhu S, Brown MF, Feller SE (2013) Retinal conformation governs pK_a of protonated Schiff base in rhodopsin activation. J Am Chem Soc 135:9391–9398